

Institute of Theoretical  
and Experimental Physics  
Preprint 15-01

M.Danilov, Yu. Gilitsky, T. Kvaratschellia, L.Laptin, I.Tichomirov,  
M.Titov, Yu.Zaitsev

**Aging Studies of Large Area Proportional  
Chambers under High-Rate Irradiation  
with  $CF_4$ -based Mixtures (PART 1).**

**PART 1**

**Moscow 2001**

Experimental conditions at the HERA-B experiment impose very strong requirements for gaseous detectors. The charged particle fluxes through the HERA-B tracking system, varying with the radial distance  $R$  from the beam line, are about  $2 \times 10^7/R^2$  particles per second, and comparable to those that will be encountered by LHC experiments.

The severe radiation environment of the HERA-B experiment leads to a maximum charge deposit on a wire, within the muon detector, of 200 mC/cm per year. We report recent results of aging studies performed by irradiating proportional wire chambers filled with  $Ar/CF_4/CH_4$  (74:20:6),  $Ar/CF_4/CH_4$  (67:30:3),  $Ar/CF_4/CO_2$  (65:30:5),  $Ar/CF_4$  (70:30),  $CF_4/CH_4$  (90:10),  $CF_4/CH_4$  (80:20) mixtures in a three different experimental setups. The size of the irradiation zone varied in the tests from 1 cm up to 500 cm. Our experience shows that the aging rate depends not only on the total collected charge, but, in addition, on the mode of operation and area of irradiation. The possible application of these results to the construction of a large area gaseous detectors for operation in high rate environments is presented.

# 1 Introduction

The HERA-B experiment is a hadronic B-factory at DESY, where B-mesons are produced via interactions of 920 GeV beam halo protons with an internal target [1, 2]. In order to reach the necessary production rate of  $b$ -quarks, the HERA-B detector must operate at an extremely high interaction rate of  $\sim 40$  MHz, corresponding to an average of 4 superimposed interactions per HERA proton bunch crossing. Such a high rate of inelastic interactions results in events with large charge and neutral multiplicities - up to several hundred particles every 96 ns - and a harsh radiation environment for the constituent detectors. The peak integrated doses in the HERA-B tracking system are about 1 Mrad/year for the Inner Tracker and  $500 \frac{mC}{cm \text{ wire}}$  per year for the Outer Tracker.

The high irradiation levels in HERA-B led to several painful experiences with aging problems in gaseous detectors. Although irradiation of small area chambers with X-rays showed that the original Inner and Outer Tracker prototype chambers are able to tolerate very large X-rays doses, corresponding to several years of operation without visible aging effects, in the HERA-B environment both chambers died within hours. In a subsequent extended R&D program these problems were solved, either by going to a revised design of the Inner Tracker (e.g. introducing GEM foils in the original diamond coated MSGC) [3, 4, 5] or by changing the original concept for the drift tubes of the Outer Tracker (surface conductivity, gas mixture, production materials) [6, 7, 8, 9].

Strong restrictions on the gas choice are imposed by the operating conditions in the muon detector (the maximum accumulated charge on the wire can reach  $200 \frac{mC}{cm \text{ wire}}$  per year). In a previous paper [10], studies of the aging performance of muon proportional chambers under sustained irradiation with  $Fe^{55}$  and  $Ru^{106}$  sources and in a 100 MeV  $\alpha$ -beam were presented. Despite the negligible gas gain loss measured after the long-term irradiation with radioactive source, rapid aging effects during irradiation with the 100 MeV  $\alpha$ -particles were observed in an  $Ar/CF_4/CH_4$  (74:20:6) mixture. From these results it

is evident that from the accumulated charge alone, it is difficult to combine the data from the different radiation sources into one consistent model. The difference between these results could be partially attributed to the type of ionization particles, the size of the irradiation area, gas gain, gas flow rate or some other variations in the operating parameters. As long as the data from different aging setups can not be combined properly, it is very difficult to give an extrapolation about the lifetime of the real detector. Therefore, we have tested the aging performance of muon proportional chambers filled with  $Ar/CF_4/CH_4$  (74:20:6),  $Ar/CF_4/CH_4$  (67:30:3) and  $Ar/CF_4/CO_2$  (65:30:5),  $Ar/CF_4$ (70:30),  $CF_4/CH_4$ (90:10),  $CF_4/CH_4$ (80:20) mixtures in the HERA - B environment, under conditions as close as possible to the real ones. The results of these aging tests are summarized in this paper.

## 2 Aging Studies in a HERA-B Environment

### 2.1 Experimental Setup

Three different types of gas proportional chambers make up the muon system: tube, pad and pixel [2]. In the following we report on aging studies performed with aluminum proportional tube chambers in the real HERA-B environment.

The main objective of these tests was to prove that muon chambers are capable of operating after exposure to an integrated charge of  $600 \frac{mC}{cm \text{ wire}}$ , which is expected after three years of operation in the hottest region, without loss in performance.

The tube chamber is a closed-cell proportional wire chamber made from an aluminum profile (wall thickness 2 mm) with a drift cell  $14 \times 12 \text{ mm}^2$  in cross section. Fig. 1 shows a schematic drawing of a tube chamber. A gold-plated tungsten wire of  $45 \mu\text{m}$  diameter and a length of nearly 3 m is stretched inside each cell and fixed mechanically with pins at the chamber endcaps.

In order to test the aging properties under conditions as close as possible to real ones, three tube chambers with 16 drift cells each and a cross section exactly as for the production version, but of a shorter length of 50 cm, were placed between the electromagnetic calorimeter and the muon absorber in the HERA-B experiment, where the charged and neutral particle fluxes are extremely high [2]. Initially, two of the chambers filled with  $Ar/CF_4/CH_4$  (67:30:3) and  $Ar/CF_4/CO_2$  (65:30:5) mixtures were subdivided to allow groups of anode wires (zones) to be operated at five different high voltages. Fig. 2 shows a simple schematic representation of the experimental

setup, numbering scheme for the wires, and summarizes the operating conditions. The applied voltages were chosen in a way to obtain comparable accumulated charges in zones 2,3,4,5. Between any two zones there was a reference wire for which high voltage was not applied. The total collected charge in each HV zone was determined by integrating the continuously recorded anode current. Due to variations in the rate of  $pN$ -interactions in the HERA-B experiment, the radiation intensity and thus the average current varied during the studies by a factor of 4, thus excluding a possibility to investigate the aging behavior as a function of rate. It should also be noted that tests with  $Ar/CF_4/CH_4$  and  $Ar/CF_4/CO_2$  mixtures have been done at about one order of magnitude higher radiation levels than expected in the muon detector (20 nA/cm), thus allowing a study of the aging properties of the gases in a more severe radiation environment. The third chamber was subdivided into 4 zones, each containing two or three wires, as shown in Fig. 2. Radiation studies with mixtures  $CF_4/CH_4$  (90:10),  $CF_4/CH_4$  (80:20),  $Ar/CF_4$  (70:30) were performed on different chamber wires in order to investigate the influence of materials and possible trace contaminants in the gas system, as well as water addition and cathode cleanliness, on the aging performance.

For each chamber a pre-mixed gas was transported by a 150 m stainless steel tube followed by a polyamid tube connected directly to the chamber inlet. The addition of water to the gas was done indirectly, by varying the length of the polyamid tube, which is transparent to  $H_2O$ , for a fixed flow rate. The gas flow within the chamber was serial: the gas inlet was connected to chamber cell N1, and the gas outlet to cell N16. The gas outlet of the chamber was connected via a 50 m stainless steel tube to the input of a gas chromatograph, which was used to analyze the concentration of species ( $Ar$ ,  $CF_4$ ,  $CH_4$ ,  $CO_2$ ,  $N_2$ ,  $O_2$ ,  $H_2O$ ) in the effluent gas stream. Usually, measured concentrations of  $N_2$  and  $O_2$  were at the level of 150-250 ppm.

Periodically (typically once/month) chamber characteristics were studied in a 3 GeV electron beam with an intensity  $\sim 1 \text{ kHz/cm}^2$ . A reduction in efficiency measured with electrons at different positions along the wire was used as the main information about the loss in performance. In addition, during irradiation in the HERA-B environment several other types of performance degradation with distinct symptoms also indicate the appearance of aging effects: dark current, special 'switch-on' current behavior (decrease in the anode current after high voltage is applied, since a certain time is necessary to establish the equilibrium charge density on the aged wire surface). This phe-

nomena has been widely described in the literature [11, 12, 13]. And finally, an interesting phenomena was observed for all aged wires operated with an  $Ar/CF_4/CH_4$  mixture: the operating current was dependent upon the gas flow rate (an increase of gas flow led to an increase in the anode current). We will come back to the experimental study of this specific aging phenomena in a subsequent paper [14]. At the same time, for all wires without gain reduction, neither 'switch-on' current behavior nor dependence of operating current upon the flow rate have been observed. Thus, the appearance of any type of performance degradation for a particular group of anode wires could also serve as a manifestation of aging effects.

Before the start of the aging run, tube chamber efficiency and singles counting rate as a function of high voltage were measured for different gas mixtures in the electron beam (see Fig. 3a,b). The readout of the chambers is based on the ASD-8 amplifier shaper discriminator chip [15]. Therefore, real after-pulses and multiple hits coming from ASD-8 per signal both contribute to the rise in singles rate curves, above the nominal beam intensity, with increasing high voltage. According to results reported in [16], operating voltages for the tube chamber were chosen for the following:  $Ar/CF_4/CH_4$  (74:20:6) - 2.25 kV,  $Ar/CF_4/CH_4$  (67:30:3) - 2.45 kV,  $Ar/CF_4/CO_2$  (65:30:5) - 2.4 kV, corresponding to the baseline gas amplification  $\sim 3 \cdot 10^4$ .

## 2.2 Aging in an $Ar/CF_4/CH_4$ (67:30:3) gas mixture

Radiation tests with an  $Ar/CF_4/CH_4$  (67:30:3) mixture, which is similar to  $Ar/CF_4/CH_4$  (74:20:6), have been carried out in the real HERA-B environment. Due to the reduced  $CH_4$  content in  $Ar/CF_4/CH_4$  (67:30:3), better aging properties of this mixture were expected. This was also confirmed during irradiation with a  $Ru^{106}$  source, where stable operation up to a total collected charge of  $2 \frac{C}{cm \text{ wire}}$  was achieved [10]. Since water added to the mixture in small concentrations is believed to prevent polymerization of hydrocarbons, we used 500 ppm of  $H_2O$  from the beginning of the tests. Typically, a chamber was flushed at a flow rate of 3 liters/hour, corresponding to two volume exchanges per hour.

First results in the HERA-B environment showed that aging effects in the  $Ar/CF_4/CH_4$ (67:30:3) + 500 ppm of  $H_2O$  mixture depend on the gas amplification (high voltage) and the size of the irradiation area.

After 10 days of exposure which resulted in a collected charge of  $\sim 25 \frac{mC}{cm \cdot wire}$  electron beam tests showed gain reduction for two (N14,N15) from three wires

operated at high voltage 2.65 kV. After an accumulated charge of  $\sim 100 \frac{mC}{cm \cdot wire}$  all three wires (N13,N14,N15) in zone 5 were already inefficient. A similar aging behavior has been observed for the wires irradiated at 2.6 kV, however their lifetime was slightly longer. After an accumulated charge of  $\sim 80 \frac{mC}{cm \cdot wire}$ , gain reduction has been found for one wire N11 and approximately at a dose of  $170 \frac{mC}{cm \cdot wire}$  electron beam tests revealed efficiency loss in both cells (N10,N11). In addition to a gain reduction for the wires irradiated at 2.6 kV and 2.65 kV, operation of these cells in the HERA-B environment was accompanied by the 'switch-on' current behavior and the appearance of the dependence of the operating current on the gas flow rate. Dark current (or Malter effect) in these zones also started to appear and could lead to a subsequent detector degradation.

It has to be noted that the efficiency loss for wires operated at 2.6 kV and 2.65 kV was more severe in the direction of the serial gas flow. Initially aging effects in zones 4 and 5 appeared on the last wires (N11,N15) in the serial gas flow, although the radiation intensity for these wires was the lowest in each zone. Fig. 4 shows an example of how the efficiency profile developed in the direction of gas flow for wire N11 with the accumulated charge. The loss in performance for cell N11 with increasing 'usage' of the gas is obvious. Wires (N13,N14,N15) were irradiated up to a dose of  $\sim 200 \frac{mC}{cm \cdot wire}$ , while aging tests in zones 2,3,4 were continued up to collected charge  $\sim 400 \frac{mC}{cm \cdot wire}$ . Due to the smaller current density the total accumulated charge in zone 1 was only  $\sim 100 \frac{mC}{cm \cdot wire}$ . We did not observe any onset of dark current in cells N1-N8 during the whole period of irradiation. After the aging run, the chamber performance was studied in an electron beam. All wires operated at 2.6 kV, 2.65 kV showed strong anode aging. At the same time, scanning along the wires N5,N7,N8 with an electron beam revealed several distinct spots with a typical size of several *cm*, where local inefficiencies were detected (measured efficiency at 2.4 kV was  $\sim 90-98 \%$ ). No change in performance was found for wires N1,N2 (2.25 kV), N4 (2.5 kV), and all reference wires.

In addition to measurements in the electron beam, at the conclusion of the run wires irradiated at 2.6 kV and 2.65 kV were taken for surface analysis at 'Digital Analytical Scanning Microscope JSM-6400'. The scanning electron microscope (SEM) yields information on the morphology of the wire surface by imaging with scattered and secondary electrons, and energy dispersive X-ray spectroscopy (EDX) analysis gives the atomic composition of the surface material. Usually, micrographs of anode wires were taken at SEM accelerat-

ing voltage 20 kV (sometimes - 5 kV), while cathodes were analyzed at 5 kV. The increased sensitivity to surface deposits at 5 kV is due to the reduced penetration of the lower energy primary electrons. Fig. 5 shows SEM micrographs and EDX analysis of wire N13 specimen taken near the gas inlet and wire N15 specimen taken near the gas outlet (150 cm downstream from the beginning of zone 5 in the serial gas flow). EDX analysis of these specimens confirmed the presence of polymers on the wires, containing carbon and fluorine as the only detectable elements (SEM is insensitive to hydrogen) (see Fig. 5). Moreover, analysis of the wires (N13,N14,N15) have shown that the  $F/C$  ratio in the surface deposit increases in the direction of the serial gas flow. SEM micrograph of wire N11 irradiated at 2.6 kV was also taken and is shown in Fig. 6. In the whisker emission 'EDX' spectrum there were identified lines corresponding only to  $C$  and  $F$  elements.

At this point we decided to study the influence of water on aging performance and continued tests with an increased  $H_2O$  content (1400 ppm), while using the previously irradiated wires in zones 1,2,3. During three months of operation, approximately  $400 \frac{mC}{cm \cdot wire}$  were accumulated for wires irradiated at 2.5 kV and 2.55 kV and  $\sim 100 \frac{mC}{cm \cdot wire}$  for wires at 2.25 kV in addition to those collected in the previous run, which resulted in a total radiation dose of  $\sim 800 \frac{mC}{cm \cdot wire}$  in zones 2,3 and  $\sim 200 \frac{mC}{cm \cdot wire}$  in zone 1. Further scanning along the wires with an electron beam have shown that small inefficient spots on wires N5,N7,N8 had vanished, and all wires became fully efficient again. No change in performance was also observed for wires N1,N4. At the same time, an efficiency drop was detected for one of the wires, N2, operated at 2.25 kV, being more severe near the chamber endcaps (measured efficiency at 2.4 kV was  $\sim 85$  %) than in the center of the wire ( $\sim 97$  %), where the radiation intensity was the largest. Upon completion of the beam studies, all wires from the chamber were analyzed under the electron microscope. EDX analysis of irradiated wires N1,N4,N5,N7,N8 and all reference wires revealed only  $Au$  peaks thus confirming the absence of the polymer coating. Fig. 7 shows the SEM micrograph and EDX spectrum for wire N5. However, SEM imaging of wire N2 revealed a surface deposit consisting of traces of  $Si$  and  $O$  (see Fig. 7). The absence of  $Si$ -containing deposits on all other aged wires operated with  $Ar/CF_4/CH_4$  indicates that  $Si$ -polymerization was not a dominant aging process in our tests, and particularly for cell N2 could be a result of contamination from chamber endcaps. Moreover, gaseous discharges in an  $Ar/CF_4/CH_4$  mixture could provide additional resistance for  $Si$ -deposits,



which react with fluorine radicals to form volatile  $SiF_4$ . In plasma polymerization, discharges of  $CF_4/H_2$  mixtures are successfully used for  $SiO_2$  etching, while  $CF_4/O_2$  plasmas selectively etches  $Si$  [17].

In order to study the influence of water on aging performance in  $Ar/CF_4/CH_4$ , we have carried out new radiation tests. For this all chamber cells were restrung with new wires. With an electron beam rate of  $1\text{ kHz/cm}^2$ , no difference in efficiency between previously irradiated and reference cells was found. However, the dark current observed in the previous run from wires N10,N11,N13,N14,N15 indicates that surface deposits could be present on the cathodes in these cells. Although a subdivision of anode wires into 4 high voltages groups was slightly changed for this run: zone 1 (wires N1,N2) - 2.25 kV, zone 2 (wires N4,N5,N6) - 2.5 kV, zone 3 (wires N8,N9) - 2.6 kV, zone 4 (wires N14,N15,N16) - 2.65 kV, this did not affect significantly the average current density in each zone. Initially, radiation tests with the previously used mixture  $Ar/CF_4/CH_4$  (67:30:3) + 1400 ppm of  $H_2O$  were performed up to radiation doses:  $40\frac{mC}{cm\cdot wire}$  in zone 1,  $80\frac{mC}{cm\cdot wire}$  in zone 2,  $100\frac{mC}{cm\cdot wire}$  in zone 3,  $120\frac{mC}{cm\cdot wire}$  in zone 4. During the whole period of irradiation, we observed dark current for the wires operated at 2.65 kV. At this point all polyamid tubes were exchanged with stainless-steel lines, thus excluding the presence of water in the chamber. Several types of performance degradation (dark current, steadily decreasing anode current) started to appear for wires operated at 2.5 kV, 2.6 kV, 2.65 kV at a level of an accumulated charge  $\sim 15\text{-}30\frac{mC}{cm\cdot wire}$ . These results were especially surprising for wires irradiated at 2.5 kV, since no gain reduction has been observed up to  $800\frac{mC}{cm\cdot wire}$  in  $Ar/CF_4/CH_4$  (67:30:3) mixture with 500 ppm and 1400 ppm of  $H_2O$ . At the end of the aging run without water, the following radiation doses were collected:  $20\frac{mC}{cm\cdot wire}$  in zone 1,  $70\frac{mC}{cm\cdot wire}$  in zone 2,  $85\frac{mC}{cm\cdot wire}$  in zone 3,  $65\frac{mC}{cm\cdot wire}$  in zone 4. (High voltage in zone 4 was switched off earlier than in other zones). It might be noted that in sharp contrast to wires in other zones no performance degradation for wires in zone 1 was observed up to the end of the run.

Studies of chamber efficiency in an electron beam confirmed significant gain reduction for all wires operated at 2.5 kV, 2.6 kV, 2.65 kV. Moreover, a strongly nonconductive polymer coating present on the wires complicated the measurement of efficiency due to the time-dependent amplitude suppression resulting from charging-up of aged wire surfaces [11]. When the chamber was opened for inspection, dark whiskers randomly distributed on all irradiated wires in zones 2,3,4 were observed. Fig. 8 presents typical micrographs of

the shaped growth deposits revealed by SEM on the wires N5 (2.5 kV) and N9 (2.6 kV), which are very similar to those observed after irradiation with  $Ar/CF_4/CH_4$  (67:30:3) + 500 ppm  $H_2O$ . The structure of these 'whiskers' suggests that they are caused by debris attaching to the anode wire and could serve as nucleation points for further deposits. It is also important to note that the deposit thickness was clearly irregular, with some areas appearing relatively clean while others had 'whisker' type deposits. Moreover, even in the 'whiskers' free region, surface deposits consisting of  $C$  and  $F$  elements and masking the underlying gold signal, were identified (see Fig. 8). Scanning along wires N1,N2 irradiated at 2.25 kV, revealed a loss in efficiency for wire N1 with a maximum drop in the center of the wire (measured efficiency at 2.4 kV was  $\sim 93\%$ ), where the radiation intensity was the largest. No change in performance was observed for wire N2. In contrast to results in other zones, these data demonstrate a dependence of the degree of aging on the irradiation intensity, and thus the accumulated charge, and not on the direction of the serial gas flow. SEM analysis at 20 kV of wire N1 revealed only gold, while the EDX spectrum at 5 kV is dominated by an intense  $C$  peak masking the  $Au$  signal. The different texture of the wire deposits at 5 kV and 20 kV, as a result of increased SEM sensitivity at 5 kV to the thin carbon layer, is clearly evident from Fig. 9. It is also notable that the deposits on the wire N1 are carbonaceous, without incorporation of  $F$  into the polymer structure. This is in contrast to typical deposits detected after irradiation with higher voltages.

Unfortunately, the relatively small accumulated charge in zone 1, leaves us unable to conclude whether the difference in chemical composition of polymers in zone 1 and 2-4 can be attributed to the change in the polymerization mechanism as a result of increased plasma density in the avalanche for higher voltage, or simply indicates that the polymerization in an  $Ar/CF_4/CH_4$  (67:30:3) mixture starts from the deposition of a carbon layer on the anode wire. Detailed discussion of the results presented here will be reported in a companion paper [14].

Several cathode pieces were also analyzed under the electron microscope. As can be seen from Fig. 10a, a thin deposit, consisting of  $C$ ,  $F$  and  $O$ , was detected on the irradiated  $Al$  surfaces. Fig. 10 also shows that the maximum  $F$  abundance was found on cathode cells N5 and N8, operated up to a dose  $\sim 1000 \frac{mC}{cm \cdot wire}$  in an  $Ar/CF_4/CH_4$  (67:30:3) mixture with 500 ppm of  $H_2O$ , 1400 ppm of  $H_2O$ , and without water. Analysis of cathode cell N10, after irradiation with  $Ar/CF_4/CH_4$  (67:30:3) + 500 ppm of  $H_2O$  up to  $400 \frac{mC}{cm \cdot wire}$

and cathode cell N6, after irradiation with  $Ar/CF_4/CH_4$  (67:30:3) + 1400 ppm of  $H_2O$  up to  $150 \frac{mC}{cm \cdot wire}$ , revealed a comparable  $F$  abundance. Since the operating conditions for wires N5 and N6 were nearly identical during the last run, the difference in the  $F$  abundance in these cells could be explained by the fact that polymer deposition on the  $Al$  surface in cell N5 also occurred in the previous run with water, when  $800 \frac{mC}{cm \cdot wire}$  were collected. Similar  $F$  abundances on cathode cells N6 and N10, after different accumulated charges, indicates a larger rate of fluorocarbon deposition on  $Al$  surfaces without water. However, it is not clear whether polymers deposited on the cathodes in the previous run (with 500 ppm and 1400 ppm of  $H_2O$ ) could provoke extremely rapid aging effects during operation without water, or if such an aging rate is defined solely by the kinetics of  $Ar/CF_4/CH_4$  wire avalanches without water, under particular discharge conditions.

**Our results clearly demonstrate that the addition of water to the mixture  $Ar/CF_4/CH_4$  (67:30:3) substantially increases the lifetime of the aluminum proportional chambers and decreases the rate of polymer deposition on the anode wires and cathode surfaces. Although under some conditions (gas gain  $< 10^5$ , water addition  $> 1000$  ppm, gas flow 3 l/h) tube chambers can be operated up to a nominal lifetime ( $600 \frac{mC}{cm \cdot wire}$ ), the strong dependence of aging properties on high voltage and size of irradiation area completely ruled out the  $Ar/CF_4/CH_4$  (67:30:3) mixture as a candidate for operation in the muon chambers at the HERA-B experiment.**

### 2.3 Aging in an $Ar/CF_4/CO_2$ (65:30:5) gas mixture

Our intensive aging studies have shown that both  $Ar/CF_4/CH_4$  (74:20:6) and  $Ar/CF_4/CH_4$  (67:30:3) mixtures failed to fulfill radiation hardness requirement and can not be used for operation in the muon detector. In order to test the suitability of the  $Ar/CF_4/CO_2$  (65:30:5) + 1000 ppm of  $H_2O$  mixture, radiation studies were performed at five different high voltages (gas gain ranges from  $10^4$  to  $3 \cdot 10^5$ ). We have employed a gas flow rate of 3 l/hour, corresponding to 2 volume exchanges per hour.

No change in performance of aluminum proportional chambers operated with  $Ar/CF_4/CO_2$  (65:30:5) + 1000 ppm mixture has been observed during the whole run up to collected charge  $\sim 700 \frac{mC}{cm \cdot wire}$  in zones 2-5. (The accumulated charge for the wires in zone 1 was  $\sim 170 \frac{mC}{cm \cdot wire}$ ). Fig. 11 shows efficiency profiles along wires N5, N10, N13 after an accumulated charge of  $700 \frac{mC}{cm \cdot wire}$  in

the  $Ar/CF_4/CO_2$  (65:30:5) + 1000 ppm mixture.

At the conclusion of these tests, the tube chamber was opened for inspection. Fig. 12 shows typical SEM micrographs of the wires irradiated at high voltages: 2.5 kV (wire N5), 2.6 kV (wire N10), 2.65 kV (wire N13). Although SEM imaging revealed some local deterioration of the smooth wire surface after a long-term operation at high gain  $\sim 3 \times 10^5$  (see Fig. 12), the elemental composition of this wire is dominated by  $Au$  peak (at 20 kV SEM voltage) and there is no evidence of other chemical elements. The appearance of a few wire specimens was slightly more black than that of a new one, however detailed SEM investigation of all irradiated wires have shown apparently clean surfaces with only a few point-like deposits ( $Si, Al$ ) with typical size of 1-2  $\mu m$ , that did not result in local inefficiencies.

While SEM demonstrated the absence of polymers on the anode wires, EDX analysis revealed trace amounts of  $C$ ,  $O$  and  $F$  on the  $Al$  cathodes in cells N13, N14, N15, irradiated at 2.65 kV (see Fig. 13). For cells N7 and N8, operated with a lower voltage of 2.55 kV, the relative abundances of  $C$ ,  $O$ ,  $F$  on  $Al$  cathodes were greatly reduced. Cathodes in cells N4 and N5, operated at 2.5 kV, were almost indistinguishable from the reference ones. Such fluorocarbon films on the cathode surfaces did not lead either to dark current or to efficiency loss. The appearance of fluorocarbon deposits on irradiated cathodes in  $CF_4$ -containing mixtures has been reported in the literature. As was shown in [18], trace fluorocarbon deposits formed on cathodes after irradiation in pure  $CF_4$  resulted in a loss of gas gain, rather than in a self-sustaining discharge. Although in other tests an increased layer of fluorine and oxygen was observed on the cathode, no change in gas gain was observed during long-term irradiation [19, 21].

**Using  $Ar/CF_4/CO_2(65:30:5)$  + 1000 ppm  $H_2O$  mixture, no loss in performance of aluminum proportional chambers was observed up to collected charge  $\sim 700 \frac{mC}{cm \cdot wire}$ , whilst irradiating with different gas gains. Analysis of cathode surfaces revealed trace amounts of  $C$ ,  $O$  and  $F$  for tubes operated at high gas gain  $\sim 10^5$ , while for a baseline gain of  $3 \cdot 10^4$ , exposed cathodes were almost indistinguishable from reference ones. Therefore,  $Ar/CF_4/CO_2(65:30:5)$  + 1000 ppm  $H_2O$  mixture is currently used for the muon chamber operation.**

## References

- [1] T. Lohse *et al.*, HERA-B collaboration, An Experiment to Study CP Violation in the B System Using an Internal Target at the HERA Proton Ring, Proposal, **DESY-PRC 94/04** (1994).
- [2] E. Hartouni *et al.*, HERA-B collaboration, An Experiment to Study CP Violation in the B System Using an Internal Target at the HERA Proton Ring, Design Report, **DESY-PRC 95/01** (1995).
- [3] F. Sauli, Nucl. Instr. and Meth. **A408** 258(1998).
- [4] B. Schmidt *et al*, Nucl. Instr. and Meth. **A 419** (1998) 230-238.
- [5] T. Zeuner, Nucl. Instr. and Meth. **A 446** (2000) 324-330.
- [6] C. Stegmann, Nucl. Instr. and Meth. **A 453** (2000) 153-158.
- [7] M. Hohlmann, Nucl. Instr. and Meth. **A 461** (2001) 21-24.
- [8] H. Kolanoski, Investigation of Aging in the HERA-B Outer Tracker Drift Tubes, Proceedings of Nuclear Science Symposium and Medical Imaging Conference, 15-20 October 2000, Lyon, France.
- [9] A. Schreiner, Aging studies of drift chambers of the HERA-B outer tracker using  $CF_4$ -based gases, Dissertation, Humboldt University, (2001).
- [10] M. Danilov, L. Laptin, I. Tichomirov, M. Titov, Yu. Zaitsev, Aging tests of proportional wire chambers using  $Ar/CF_4/CH_4$  (74:20:6),  $Ar/CF_4/CH_4$  (67:30:3) and  $Ar/CF_4/CH_4$  (65:30:5) mixtures for the HERA-B Muon Detector, ITEP-43-00 (2000); hep-ex/0107080.
- [11] A. Algeri *et al*, Nucl. Instr. and Meth. **A 338** (1994) 348-367.
- [12] N. Spielberg, D. Tsarnas Rev. Sci. Instr. **Vol.46 (8)** (1975) 1086-1091.
- [13] M. Fraga *et al*, Nucl. Instr. and Meth. **A 419** (1998) 485-489.
- [14] The effect of added  $CF_4$  on aging performance of wire proportional chambers, in preparation.
- [15] M. Buchler *et al*, IEEE Trans. Nucl.Sci., **NS-46** (1999) 126-132.

- [16] S. Barsuk *et al*, A Gaseous Muon Detector at the HERA-B Experiment, IEEE Trans. Nucl.Sci., **NS-48(4)** (2001) 1059-1064.
- [17] M.J. Kushner, J. Appl. Phys, **Vol.53**, (4) (1982) 2923-2938.
- [18] J. Wise *et al*, J. Appl. Phys, **Vol.74**, (9) (1993) 5327-5340.
- [19] V. Pashhoff, Dissertation, University Freiburg, October (1999)
- [20] M. Kollfrath, Dissertation (in german), University Freiburg, (1999)
- [21] D.S. Denisov, On using  $CF_4$  as a working gas for drift tubes (in russian), IHEP-preprint-90-16 (1990)
- [22] E. Kay, Invited Pap. Int. Round Table Plasma Polym. Treat., IUPAC Symp., Plasma Chem. (1977).
- [23] H. Yasuda, Plasma Polymerization, (Academic Press, 1985)
- [24] C. Mogab *et al*, J. Appl. Phys, **Vol.49**, (7) (1978) 3796-3803.
- [25] R. Openshaw *et al*, Nucl. Instr. and Meth. **A 307** (1991) 298-308.
- [26] G. Alexeev *et al*, Technical design Report for the D0 Forward Muon Tracking Detector Based on Mini-Drift Tubes, D0 Note 3366, (1997)
- [27] L.G. Christophorou *et al*, Nucl. Instr. and Meth. **A 163** (1979) 141-149.
- [28] J. Fischer *et al*, Nucl. Instr. and Meth. **A 238** (1979) 249-264.
- [29] B. Schmidt, S. Polenz Nucl. Instr. and Meth. **A 273** (1988) 488-493.
- [30] L.G. Christophorou *et al*, J. Phys. Chem. Ref. Data, **Vol.25**, **No.5** (1996) 1341-1388.
- [31] J. Kadyk *et al*, IEEE Trans. Nucl. Sci **NS-37** (2) (1990) 478-486.
- [32] R. Openshaw *et al*, Nucl. Instr. and Meth. **A 307** (1991) 298-308.
- [33] Proc. Workshop on Radiation Damage to Wire Chambers, Lawrence Berkeley Laboratory (Jan. 1986) LBL-21170.
- [34] J. Va'vra, ref. [33], pp. 263-294.
- [35] J. A. Kadyk, Nucl. Instr. and Meth. **A 300** (1991) 436-479.
- [36] T. Arikado, Ya. Horiike, Jpn. J. Appl. Phys, **Vol.22**, (5) (1983) 799-802.

- [37] J.C. Martz *et al*, J. Appl. Phys, **Vol.67**, (8) (1990) 3609-3617.
- [38] E. Truesdale, G. Smolinsky, J. Appl. Phys, **Vol.50**, (11) (1979) 6594-6599.
- [39] E. Truesdale *et al*, J. Appl. Phys, **Vol.51**, (5) (1979) 2909-2913.
- [40] A. Romaniouk, Choice of materials for the constructio of TRT, ATLAS Internal Note, INDET-98-211 (1998)

Figure 1: Schematic drawing of the single layer tube chamber. Dimensions are indicated in units of mm.

Figure 2: Schematic representation of the experimental system and numbering scheme for wires in the chamber. Operating conditions (high voltage and average current density) in each zone are also indicated.

Figure 3: a) Tube chamber efficiency as a function of high voltage; b) Singles counting rate as a function of high voltage.

Figure 4: Efficiency profiles along wire N11 for three different accumulated charges:  $80 \frac{mC}{cm \cdot wire}$ ,  $170 \frac{mC}{cm \cdot wire}$ ,  $270 \frac{mC}{cm \cdot wire}$ , measured in an electron beam at 2.4 kV with  $Ar/CF_4/CH_4$  (67:30:3) mixture. These results are to be compared with the efficiency of reference wires  $> 99\%$  at 2.4 kV.

Figure 5: SEM micrographs and EDX analysis of wire N13 specimen taken near the gas inlet and wire N15 specimen taken near the gas outlet (150 cm downstream from the beginning of zone 5 in the serial gas flow).

Figure 6: SEM micrograph of wire N11 irradiated at 2.6 kV. After a dose of  $400 \frac{mC}{cm \cdot wire}$  in an  $Ar/CF_4/CH_4$  (67:30:3) + 500 ppm  $H_2O$  mixture, wire showed strong anode aging. EDX spectrum is taken from the place marked with the box.

Figure 7: SEM micrographs and EDX spectra for wires N2 and N5 irradiated at 2.25 kV (2.5 kV) up to radiation doses  $\sim 200 \frac{mC}{cm \cdot wire}$  ( $\sim 800 \frac{mC}{cm \cdot wire}$ ) in an  $Ar/CF_4/CH_4$  (67:30:3) mixture with 500 ppm and 1400 ppm  $H_2O$ .

Figure 8: Typical deposits ('whiskers') on the anode wires N5 (2.5 kV) and N9 (2.6 kV) after irradiation in an  $Ar/CF_4/CH_4$  (67:30:3) mixture. Even in the 'whiskers' free region, surface deposit is present, as can be evident from the EDX spectrum taken in the place marked with box.

Figure 9: SEM micrographs of wire N1, irradiated in an  $Ar/CF_4/CH_4$ (67:30:3) mixture with 1400 ppm  $H_2O$  and without water up to an accumulated charge of  $60 \frac{mC}{cm \cdot wire}$ , show the different EDX sensitivity at 5 kV and 20 kV.



Figure 10: EDX spectroscopy of the cathodes in cells N5,N6,N8,N10. A thin deposit, consisting of  $C$ ,  $F$  and  $O$ , was detected on the irradiated  $Al$  surfaces.

Figure 11: Efficiency profiles along wires N5,N10,N13, measured in an electron beam at 2.35 kV, after an accumulated charge of  $700 \frac{mC}{cm \cdot wire}$  in the  $Ar/CF_4/CO_2$  (65:30:5) + 1000 ppm of  $H_2O$  mixture. These results are to be compared with efficiency of reference wires  $> 99\%$  at 2.35 kV.

Figure 12: SEM imaging of the wires irradiated at high voltages: 2.5 kV (wire N5), 2.6 kV (wire N10), 2.65 kV (wire N13) up to a dose  $\sim 700 \frac{mC}{cm \cdot wire}$ . Despite some local deterioration of the smooth wire surface N13, the EDX spectrum at 20 kV is dominated by  $Au$  peak.

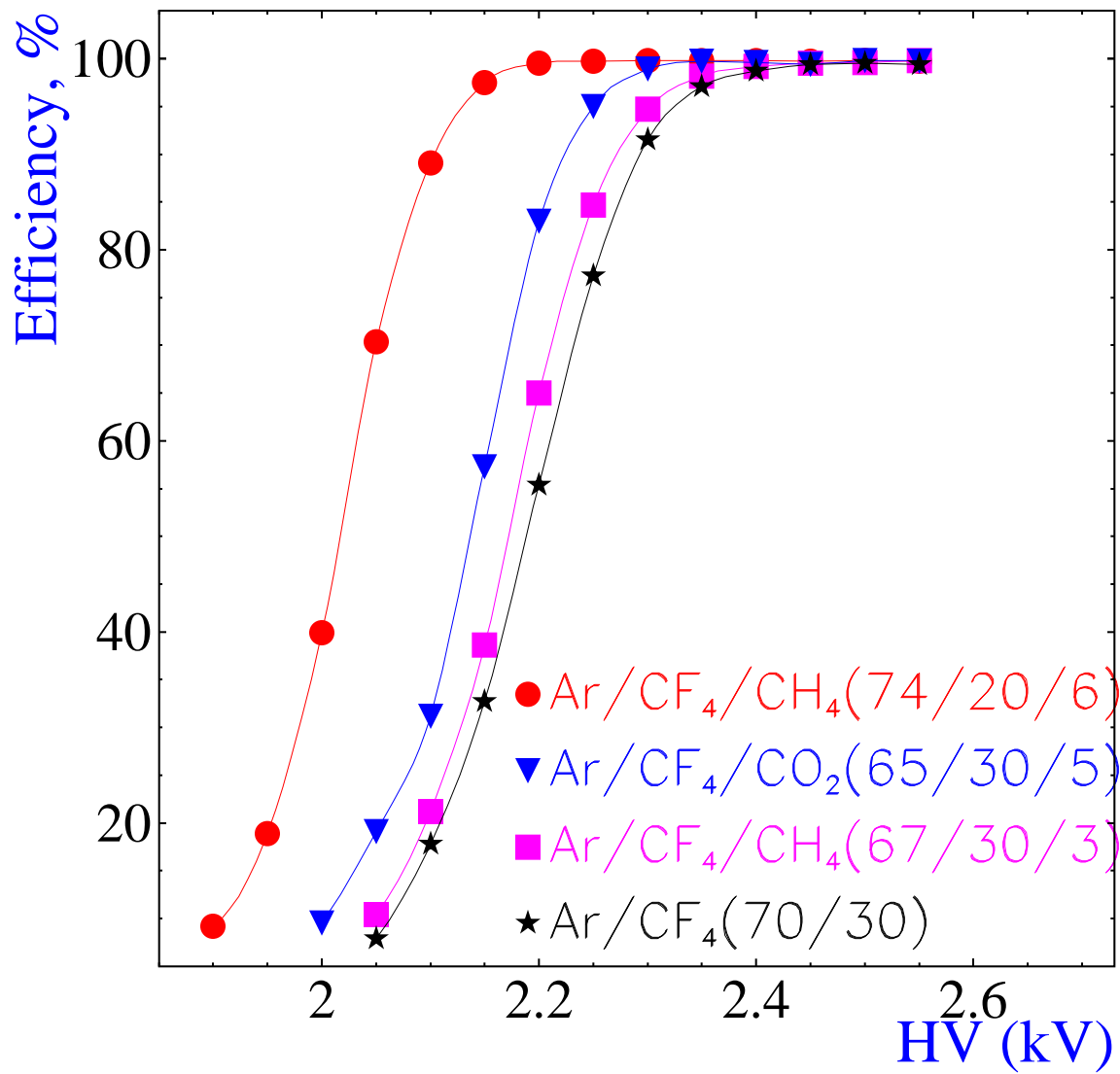
Figure 13: EDX spectroscopy of the 'reference cell' cathode (N3) and cathodes irradiated at high voltages: 2.5 kV (N5), 2.55 kV (N8), 2.65 kV (N13) up to a dose  $\sim 700 \frac{mC}{cm \cdot wire}$  in an  $Ar/CF_4/CO_2$  (65:30:5) + 1000 ppm of  $H_2O$  mixture.

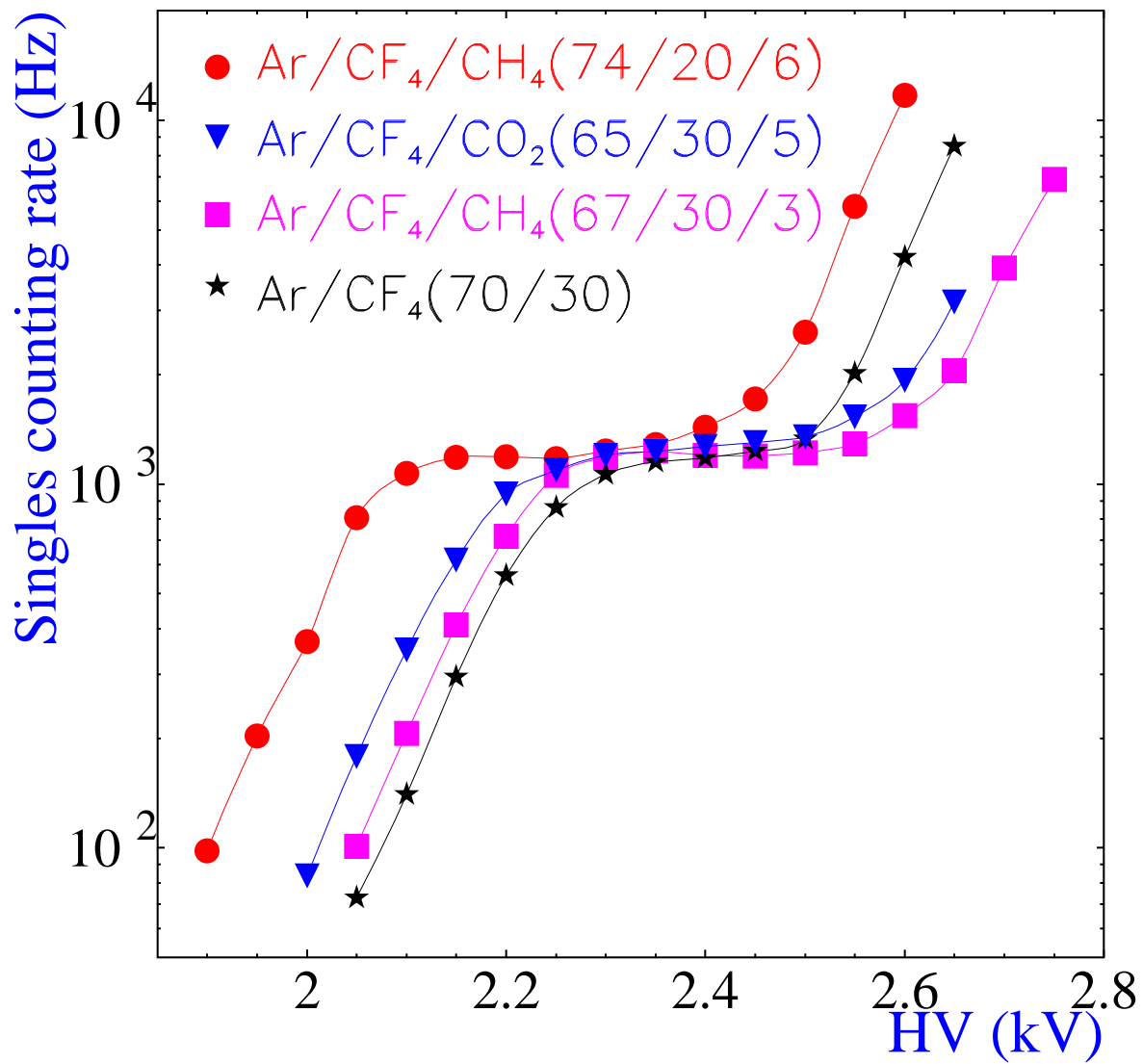
This figure "Fig1.jpg" is available in "jpg" format from:

<http://arxiv.org/ps/hep-ex/0111078v1>

This figure "Fig2.jpg" is available in "jpg" format from:

<http://arxiv.org/ps/hep-ex/0111078v1>





This figure "Fig4.jpg" is available in "jpg" format from:

<http://arxiv.org/ps/hep-ex/0111078v1>

This figure "Fig5.jpg" is available in "jpg" format from:

<http://arxiv.org/ps/hep-ex/0111078v1>

This figure "Fig6.jpg" is available in "jpg" format from:

<http://arxiv.org/ps/hep-ex/0111078v1>



This figure "Fig7.jpg" is available in "jpg" format from:

<http://arxiv.org/ps/hep-ex/0111078v1>

This figure "Fig8.jpg" is available in "jpg" format from:

<http://arxiv.org/ps/hep-ex/0111078v1>

This figure "Fig9.jpg" is available in "jpg" format from:

<http://arxiv.org/ps/hep-ex/0111078v1>

This figure "Fig10.jpg" is available in "jpg" format from:

<http://arxiv.org/ps/hep-ex/0111078v1>

This figure "Fig11.jpg" is available in "jpg" format from:

<http://arxiv.org/ps/hep-ex/0111078v1>

This figure "Fig12.jpg" is available in "jpg" format from:

<http://arxiv.org/ps/hep-ex/0111078v1>

This figure "Fig13.jpg" is available in "jpg" format from:

<http://arxiv.org/ps/hep-ex/0111078v1>